

On-chip quantum interference between silicon photon-pair sources

J. W. Silverstone^{1*}, D. Bonneau^{1*}, K. Ohira², N. Suzuki², H. Yoshida², N. Iizuka², M. Ezaki², C. M. Natarajan³, M. G. Tanner⁴, R. H. Hadfield⁴, V. Zwiller⁵, G. D. Marshall¹, J. G. Rarity¹, J. L. O'Brien¹, M. G. Thompson¹

¹Centre for Quantum Photonics, H. H. Wills Physics Laboratory & Department of Electrical and Electronic Engineering, University of Bristol, Merchant Venturers Building, Woodland Road, Bristol BS8 1UB, UK.

²Corporate Research & Development Center, Toshiba Corporation, 1, Komukai Toshiba-cho, Saiwai-ku, Kawasaki 212-8582, Japan.

³E. L. Ginzton Laboratory, Stanford University, Stanford 94305, USA.

⁴School of Engineering, University of Glasgow, Glasgow G12 8QQ, UK.

⁵Kavli Institute of Nanoscience, TU Delft, 2628CJ Delft, The Netherlands

* Authors J.W.S. and D.B. contributed equally to this work.

arXiv:1304.1490v3 [quant-ph] 20 Nov 2014

Large-scale integrated quantum photonic technologies^{1,2} will require the on-chip integration of identical photon sources with reconfigurable waveguide circuits. Relatively complex quantum circuits have already been demonstrated³⁻⁷, but few studies acknowledge the pressing need to integrate photon sources and waveguide circuits together on-chip^{8,9}. A key step towards such large-scale quantum technologies is the integration of just two individual photon sources within a waveguide circuit, and the demonstration of high-visibility quantum interference between them. Here, we report a silicon-on-insulator device combining two four-wave mixing sources, in an interferometer with a reconfigurable phase shifter. We configure the device to create and manipulate two-colour (non-degenerate) or same-colour (degenerate), path-entangled or path-unentangled photon pairs. We observe up to $100.0 \pm 0.4\%$ visibility quantum interference on-chip, and up to $95 \pm 4\%$ off-chip. Our device removes the need for external photon sources, provides a path to increasing the complexity of quantum photonic circuits, and is a first step towards fully-integrated quantum technologies.

Most quantum waveguide circuits to date have been fabricated from glass-based materials, which offer low propagation loss, a wide transparency window, and efficient coupling to optical fibre, but also limit device functionality and suffer from large circuit footprints. The silicon-on-insulator photonics platform (SOI), recently developed for classical applications^{10,11}, has several advantages over glass-based systems, including a high component density, a strong $\chi^{(3)}$ optical nonlinearity, mature fabrication techniques, fast optical modulators¹², and compatibility with both 1550-nm telecom optics and CMOS electronics. As such, SOI quantum photonic circuits¹³ and spontaneous photon-pair sources¹⁴⁻¹⁸ have recently been shown.

Our SOI photonic device is presented in Fig. 1a. Inside the device are two photon-pair sources, each comprising a 5.2-mm-long spiraled silicon waveguide in which the $\chi^{(3)}$ spontaneous four-wave mixing (SFWM) process is possible (region II, Fig. 1a). SFWM creates a signal-idler photon pair by annihilating two photons from a bright pump beam (Fig. 1b). Non-degenerate pairs are created by a single-wavelength pump, while degenerate pairs require a dual-wavelength scheme^{19,20}. In our experiments, two amplified continuous-wave lasers produced the required pump

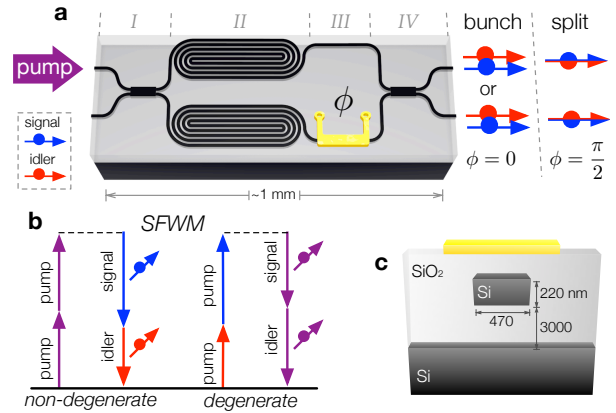


Figure 1 | Mode of operation, mechanism of photon-pair generation, and physical structure of the device. **a.** Schematic of device operation. A bright pump laser is coupled onto the silicon-on-insulator (SOI) chip using a lensed optical fibre and on-chip spot-size converters (not shown). The pump is distributed between two modes via a 2×2 multi-mode interference coupler (I), and excites the $\chi^{(3)}$ spontaneous four-wave mixing (SFWM) effect within each spiraled SOI waveguide source (II), to produce signal-idler photon pairs in the two-photon entangled state $\frac{1}{\sqrt{2}}(|20\rangle - |02\rangle)$. The pairs are thermo-optically phase shifted (ϕ , III), and interfered on a second coupler (IV) to yield either bunching or splitting over the two output modes, depending on ϕ . **b.** Energy diagrams of both types of SFWM, showing the time-reversal symmetry between the non-degenerate and degenerate processes. **c.** SOI waveguide cross-section, with thermal phase shifter on top.

field. Pump distribution and single-photon interference were achieved using 2×2 multi-mode interference couplers (MMI, reflectivity $\approx 50\%$), while a thermal phase-shifter modified the on-chip quantum and bright-light states. Off-chip wavelength-division multiplexers (WDM) were used to separate the signal, idler, and pump channels, before the photon pairs were finally measured by two superconducting single-photon detectors (dark count rate 1 kHz, gate width 650 ps).

Evolution of the degenerate quantum and bright-light states proceeded, referring to regions (I-IV) of Fig. 1a, as follows. The bright pump was equally split by the first MMI (I) between the two sources (II). By operating in the weak pump regime (so that only one pair was likely to be generated), the si-

multaneous pumping of both sources yielded a path-entangled NOON state: $\frac{1}{\sqrt{2}}(|20\rangle - |02\rangle)$. The relative phase was then dynamically controlled via a thermal phase-shifter in one arm (III), which applied a ϕ shift to the bright-light pump and a 2ϕ shift to the entangled biphoton state: $\frac{1}{\sqrt{2}}(|20\rangle - e^{i2\phi}|02\rangle)$. Finally, the bright-light and biphoton states were interfered on a second MMI (IV) to yield Mach-Zehnder interference fringes in the bright pump transmission, and half-period ($\frac{\lambda}{2}$ -like) fringes²¹ in the photon pair statistics, of the form

$$|\Psi_{\text{out}}\rangle = \cos \phi |\Psi_{\text{bunch}}\rangle + \sin \phi |\Psi_{\text{split}}\rangle. \quad (1)$$

Here, the $|\Psi_{\text{bunch}}\rangle$ state describes photons bunched together (coalesced) in either output mode A or B , and the $|\Psi_{\text{split}}\rangle$ state describes pair splitting, with one photon in each mode²⁰. By considering the *degenerate* pair case, and specifically setting $\phi = 0$ or $\phi = \frac{\pi}{2}$, we can obtain either state at the output:

$$|\Psi_{\text{out}}\rangle = \begin{cases} |\Psi_{\text{bunch}}\rangle = \frac{1}{\sqrt{2}}(|20\rangle - |02\rangle), & \text{for } \phi = 0 \\ |\Psi_{\text{split}}\rangle = |11\rangle, & \text{for } \phi = \frac{\pi}{2}. \end{cases} \quad (2)$$

When *non-degenerate* pairs are created, signal-idler exchange symmetry leads to identical quantum evolution and non-classical interference as eqs. (1,2). The corresponding $|\Psi_{\text{bunch}}\rangle$ and $|\Psi_{\text{split}}\rangle$ states for non-degenerate SFWM are:

$$\begin{aligned} |\Psi_{\text{bunch}}\rangle &= \frac{1}{\sqrt{2}} \left(|1_s 1_i\rangle_A |0_s 0_i\rangle_B - |0_s 0_i\rangle_A |1_s 1_i\rangle_B \right) \\ |\Psi_{\text{split}}\rangle &= \frac{1}{\sqrt{2}} \left(|1_s 0_i\rangle_A |0_s 1_i\rangle_B + |0_s 1_i\rangle_A |1_s 0_i\rangle_B \right), \end{aligned} \quad (3)$$

where s and i indicate signal and idler wavelengths (for more detail, see Supplementary Section S4). We will show experimentally that these *non-degenerate* colour-entangled^{22,23} states behave like *degenerate* pairs.

High-visibility quantum interference—the non-classical interference between two photons²⁴ on a beamsplitter—underpins all of photonic quantum information science and technology. Quantum interference within our device was quantified by the splitting and bunching probabilities at the output, P_{split} and P_{bunch} , as the on-chip phase (ϕ) was varied; classical interference was observed in the transmission of the bright pump through the interferometer. First, we manipulated the on-chip path entanglement of the two-colour (non-degenerate) pairs. The experimental apparatus is pictured in Fig. 2a, and detailed in Supplementary Section S1. WDMs separated the monochromatic 1549.6-nm pump from the non-degenerate signal and idler photons (detuned by $\delta = 6.4$ nm) such that signal-idler coincidences and pump transmission could be measured at the same time. Detector coincidences $A_s \times B_i$ and $B_s \times A_i$ were measured for P_{split} , while $A_s \times A_i$ and $B_s \times B_i$ were measured for P_{bunch} . The rates of classical transmission, as well as P_{split} and P_{bunch} are recorded in Figs. 2b, 2c, and 2d, respectively. In all cases, high-visibility interference was observed, and both the P_{split} and P_{bunch} two-photon fringes exhibited a phase-doubling compared to their classical counterparts—a signature of path-entangled two-photon NOON states.

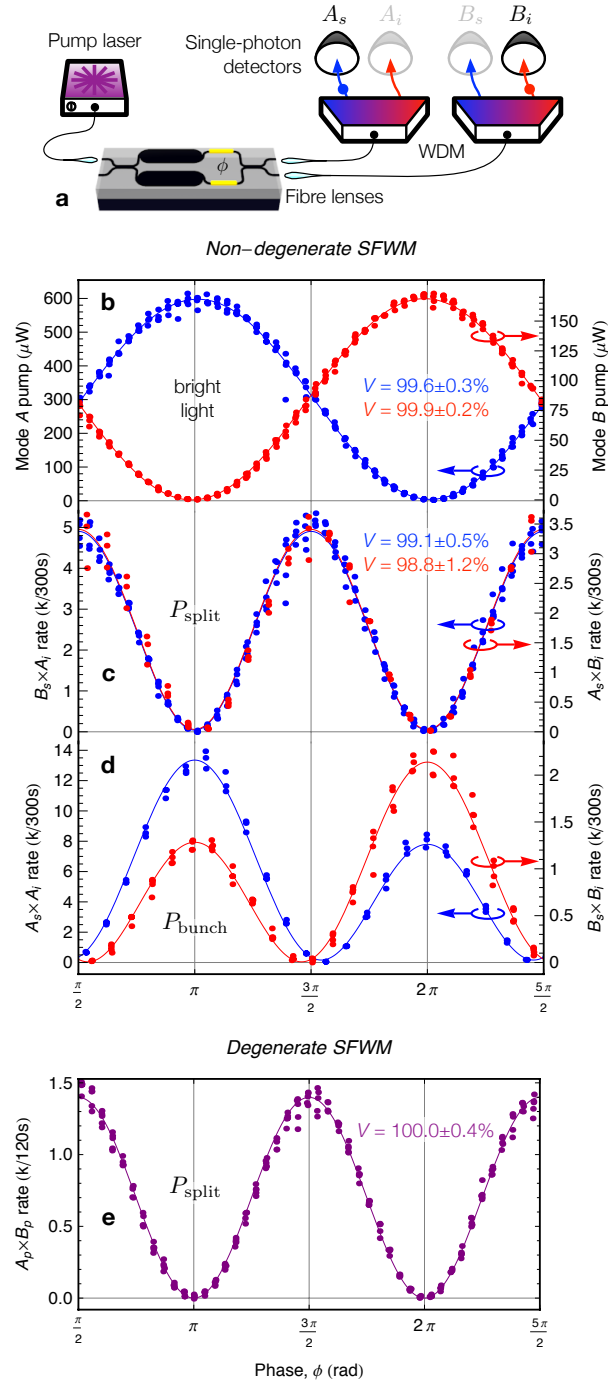


Figure 2 | On-chip quantum and classical interference measurements, varying the internal phase ϕ . Coincidence data have accidental coincidences subtracted. **a**. Apparatus, showing the coupling of light from a bright pump laser into the device, via fibre lenses, and the separation of signal (blue), idler (red), and pump (violet) wavelength channels using wavelength-division multiplexers (WDM). **b**. Transmission of the bright pump laser, showing quantum interference. **c**. Measurement of signal-idler photon splitting between modes A and B , showing quantum interference. **d**. Measurement of signal-idler photon bunching, with signal and idler both in mode A or mode B . Fringe asymmetry arises from spurious SFWM pairs generated in the input and output waveguides (see text). **e**. Photon splitting, like (b), but with monochromatic photon pairs, created via degenerate SFWM.

According to equation (1), the splitting rate should follow $P_{\text{split}} \propto \sin^2 \phi$ (curves, Fig. 2c). This model works well, with the data exhibiting net visibilities of $99.1 \pm 0.5\%$ for $A_i \times B_s$, and $98.8 \pm 1.2\%$ for $A_s \times B_i$, where we compute the visibility $V = (N_{\text{max}} - N_{\text{min}})/N_{\text{max}}$ from the maximum N_{max} and minimum N_{min} values of each fit. The uncorrected visibilities for these measurements remained around 96%—all raw visibilities, including those for the following measurements, are listed in Supplementary Section S7. Meanwhile, for the bunching rate, eq. (1) predicts $P_{\text{bunch}} \propto \cos^2 \phi$, but an asymmetric behaviour is observed instead (Fig. 2d). This behaviour can be explained by considering spurious SFWM in the device’s input and output (I/O) waveguides—identical in cross-section to the source waveguides (Fig. 1c). We calculate corrected bunching probabilities, P_{bunch}^A and P_{bunch}^B , at the two output modes A and B as,

$$P_{\text{bunch}}^B = |(\Gamma_0 + \Gamma_{\text{I/O}}) \cos \phi \mp \Gamma_{\text{I/O}}|^2 \quad (4)$$

where Γ_0 is the base SFWM rate of the spiral sources, and $\Gamma_{\text{I/O}}$ quantifies the generation rate of spurious pairs inside the I/O waveguides (see Supplementary Section S5). Equation (4) describes the P_{bunch} data well (curves, Fig. 2c). We extracted the spurious pair rate $\Gamma_{\text{I/O}}^2$, and found that such pairs accounted for a small fraction of the total: $\Gamma_{\text{I/O}}^2/\Gamma_0^2 = 2.5\%$ for P_{bunch}^A , and 2.1% for P_{bunch}^B . Since SFWM efficiency scales quadratically with interaction length ($\Gamma^2 \propto L^2$, see Supplementary Section S3), we compared these ratios with the I/O-to-source waveguide-length ratio squared, $L_{\text{I/O}}^2/L_0^2 = 2.0\%$, and found good agreement. The $\Gamma_{\text{I/O}}^2/\Gamma_0^2$ ratio is of considerable importance—it measures the amount of $|\Psi_{\text{bunch}}\rangle$ contamination when the device is configured to produce only $|\Psi_{\text{split}}\rangle$. In our experiments, spurious pairs limited the observable off-chip quantum interference visibility to $V < 98\%$ (Supplementary Section S6). This noise could be suppressed by modifying the waveguide geometry outside the source regions¹⁵, or by moving to resonant sources¹⁷.

To show how our $|\Psi_{\text{split}}\rangle$ pairs could be used in an external circuit, and to explore the implications of the colour entanglement of our non-degenerate pairs, we performed several off-chip Hong-Ou-Mandel-type (HOM) quantum interference measurements²⁵, for various values of the signal-idler detuning δ . The modified apparatus is pictured in Fig. 3a. We configured the device to generate $|\Psi_{\text{split}}\rangle$ at the chip output (by setting $\phi = \pi/2$), then sent one photon to a tunable delay line, and the other to a polarisation controller. Thus, the optical path and polarisation of the two photons could be precisely matched, and we could introduce distinguishability in the arrival time degree of freedom. The photon pairs then interfered on a fibre beamsplitter ($R = 50.2\%$), and we recorded coincidences while varying the arrival time (via the free-space displacement, x).

The phase-stable two-colour $|\Psi_{\text{split}}\rangle$ state yielded HOM interference fringes (Fig. 3b-d) which exhibited a beating between the non-degenerate signal and idler wavelengths^{22,26} (with detuning δ). Due to the colour entanglement present in $|\Psi_{\text{split}}\rangle$, the filtered biphoton spectrum has two lobes—one lobe from each of the signal- and idler-channel filters (insets Fig. 3b-d). Since the time-domain HOM interference pattern is effectively the Fourier transform of this spectrum, we can calculate the coincidence probability after the beamsplitter to be

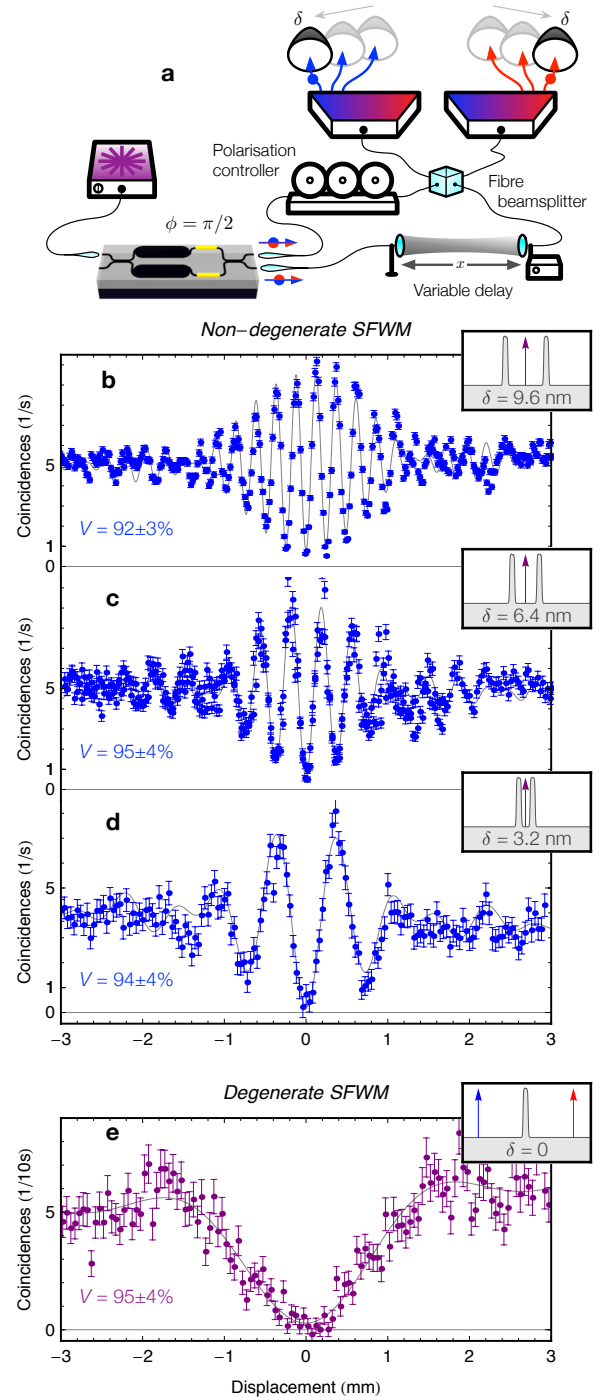


Figure 3 | Off-chip Hong-Ou-Mandel quantum interference measurements of $|\Psi_{\text{split}}\rangle$. Beating within each fringe is explained by the signal-idler detuning, δ , as plotted in insets to **b** - **e**. Coincidence data have accidental coincidences subtracted. Error bars are Poissonian, based on raw coincidences. **a**. Experimental schematic. Photon pairs in the $|\Psi_{\text{split}}\rangle$ state exit the chip, and one is delayed by a displacement x , while the other is polarisation matched, then the pair is interfered on a beamsplitter. Two detectors measure coincidences at different signal-idler detunings δ . **b**. Detuning $\delta = 9.6$ nm. **c**. Detuning $\delta = 6.4$ nm. **d**. Detuning $\delta = 3.2$ nm. **e**. Degenerate SFWM, no detuning.

$$P_{\text{HOM}} = \frac{1}{2} - \frac{V}{2} \cos\left(2\pi x \frac{\delta}{\lambda_p^2}\right) \text{sinc}\left(2\pi x \frac{w}{\lambda_p^2}\right), \quad (5)$$

where x is the delay displacement, λ_p is the pump wavelength, w is the WDM channel width, and δ is the signal-idler channel spacing. As we tuned $\delta \rightarrow 0$, the beat frequency decreased (Figs. 3b-d), as predicted by eq. (5). Off-chip HOM interference visibilities were measured for each value of δ : $V_{9.6\text{nm}} = 94 \pm 4\%$, $V_{6.4\text{nm}} = 95 \pm 4\%$, and $V_{3.2\text{nm}} = 92 \pm 3\%$. These results show that our device would perform well as an on-chip two-photon source.

Multi-photon experiments have traditionally used degenerate photon pairs at (near) visible wavelengths in discrete spatial modes to allow arbitrary multi-pair interference²⁷. As a route towards such experiments on a silicon chip at telecom wavelengths, we produced degenerate photons via *degenerate* SFWM—the time-reversed version of the non-degenerate process—which requires a two-colour pump (Fig. 1b, see Supplementary Section S1 for apparatus details). Using degenerate SFWM, with a detuning of 22.4 nm between the two pump wavelengths, we observed an on-chip quantum interference fringe with $V = 100.0 \pm 0.4$ (Fig. 2e), and measured off-chip HOM interference with $V = 95 \pm 4\%$ (Fig. 3e). The oscillation-free HOM fringe corresponded to eq. (5) with $\delta = 0$.

Using both degenerate and non-degenerate SFWM, we observed high-visibility quantum interference, both on- and off-chip (Figs. 2 and 3). We observed visibilities on-chip higher than those measured off-chip, and two explanations exist: first, as mentioned, the off-chip visibility was limited by spurious pair generation in the I/O waveguides; and second, the HOM interference measurements required both the on-chip phase, and the off-chip polarisation to be precisely controlled, and drifts in both parameters reduced the visibility. Regardless, the HOM visibilities were still high, and we view the even higher *on-chip* visibilities as showing great promise for future high-fidelity²⁸ source-circuit integrations.

Despite these high visibilities, the measured count-rates were low, due to poor system efficiency (see Methods), and low source brightness. To extract the source brightness, we examined an isolated spiral waveguide: we measured 2.7 ± 0.4 kHz/nm/mW² for non-degenerate pairs, and a similar 2.5 ± 0.6 kHz/nm/mW² for degenerate pairs, per units bandwidth and launched power. Corresponding coincidence-to-accidental ratios were 290, and 45 (at 100 kHz generation rates; see Supplementary Section S2). Brightness can be improved by: further engineering our spiral sources, i.e. optimising the spiral length; or moving to resonant^{17,29} or slow-light¹⁸ SFWM enhancement. Even with the current brightness, though, we have shown that our device can fill the on-chip role that external crystal- or fibre-based sources have traditionally taken.

Scalability is the ultimate goal for any integrated quantum system. Bulk crystal spontaneous pair sources have been used successfully in the largest optical quantum information experiments to date²⁷, including the production³⁰ and manipulation³¹ of 8-photon entanglement. These spontaneous sources can, in principle, be scaled beyond this 8-photon limit by using the techniques of active multiplexing and feed-forward^{32,33}. These schemes will require integrated fast switches, single-photon detectors, a high system efficiency, and many identical

and bright on-chip photon-pair sources. We have shown that two identical SFWM sources can be integrated monolithically in a waveguide circuit and made to interfere with high visibility. This takes us one step closer to integrated quantum circuits capable of generating and manipulating large photonic states.

Methods

System efficiency. Using the quadratic non-degenerate SFWM power dependence, we can extract the on-chip SFWM rate, together with the associated channel efficiencies, η_s and η_i , where

$$\eta_s = \frac{R_{CC}}{R_i} = -24.2 \text{ dB}, \quad \text{and} \quad \eta_i = \frac{R_{CC}}{R_s} = -25.5 \text{ dB},$$

and R_{CC} , R_i , and R_s are respectively the coincidence, idler channel, and signal channel rates. These values quantify the total loss experienced by a photon from its generation to detection at detector s or i , respectively. Both detector efficiencies were measured at 8% (−11.0 dB). From a cut-back measurement on the same wafer we estimate the propagation loss at 4.1 dB/cm, though much lower loss is possible³⁴. Using η_s and η_i , and bright-light measurements, we calculate the combined MMI and facet loss as 7.3 dB. We were unable to separate the MMI losses from those of the facet, though very low-loss MMI designs exist³⁵.

Optical apparatus. We used two continuous-wave tuneable lasers to generate the required pump field (one or two colours). These lasers were amplified by an erbium-doped fibre amplifier, to produce a total power of 80 mW (in the two-colour case, this was divided between two spectral peaks), then filtered (50 dB extinction), and the remaining 15 mW was edge-coupled onto the chip using 2.5- μm -beam-waist lensed fibres and on-chip polymer spot-size converters. Fibre alignment was maintained using piezo-controlled feedback on the bright pump transmission. Filtering was used to both clean the pump before the chip, and to separate the pump from the single photons afterwards. See Supplementary Section S1 for further details.

Off-chip HOM fringe optimisation. The apparatus was configured as in Fig. 3. We used the interferometer, formed between the chip and the fibre beamsplitter, to determine the zero-path-length-difference point on the free-space delay. We input amplified noise to this interferometer, and observed white light fringes as we varied the delay, with fringe maxima at the zero-difference point (and also the HOM fringe centre). We then optimised the polarisation controller using the classical fringe visibility.

Electrical apparatus. An electrical probe was used to electrically interface between the chip and an ultra-low noise DC power supply. We applied voltages up to 2.3 V to our thermo-optic phase modulator, for a maximum load of 36 mA. Similar devices exhibited fuse voltages around 2.7 V. We correlated electrical power with thermo-optic phase, with good results (Fig. 2b, Supplementary Figure 3).

Device fabrication. The silicon nanowire waveguides were fabricated from a silicon-on-insulator (SOI) wafer having a 220 nm slab thickness. The waveguides were designed to be single-moded, having a width of 470 nm with a silicon dioxide upper cladding. I/O coupling was achieved using spot-size converters comprising a 300- μm -long inverse-taper with a 200-nm-wide tip beneath a $4 \times 4 \mu\text{m}^2$ polyimide waveguide. Structures were defined by deep UV photolithography (248 nm) and dry etching.

References

- [1] O’Brien, J.L., Furusawa, A. & Vuckovic, J. Photonic quantum technologies. *Nature Photon.* **3**, 687-695 (2009).
- [2] Tanzilli, S. *et al.* On the genesis and evolution of integrated quantum optics. *Laser Photon. Rev.* **1**, 115-143 (2012).
- [3] Peruzzo, A. *et al.* Quantum Walks of Correlated Photons. *Science* **329**, 1500-1503 (2010).
- [4] Shadbolt, P.J. *et al.* Generating, manipulating and measuring entanglement and mixture with a reconfigurable photonic circuit. *Nature Photon.* **6**, 45-49 (2012).
- [5] Metcalf, B.J. *et al.* Multiphoton quantum interference in a multiport integrated photonic device. *Nat. Commun.* **4**, 1356 (2013).
- [6] Tillmann, M. *et al.* Experimental boson sampling. *Nature Photon.* **7**, 540-544 (2013).

- [7] Crespi, A. *et al.* Anderson localization of entangled photons in an integrated quantum walk. *Nature Photon.* **7**, 322-328 (2013).
- [8] Matsuda, N. *et al.* A monolithically integrated polarization entangled photon pair source on a silicon chip. *Sci. Rep.* **2**, 817 (2012).
- [9] Martin, A., Alibart, O., DeMicheli, M.P., Ostrowsky, D.B. & Tanzilli, S. A quantum relay chip based on telecommunication integrated optics technology. *New J. Phys.* **14**, 025002 (2012).
- [10] Soref, R. The Past, Present, and Future of Silicon Photonics. *J. Sel. Top. Quant. Electron.* **12**, 1678-1687 (2006).
- [11] Sun, J., Timurdogan, E., Yaacobi, A., Hosseini, E.S. & Watts, M.R. Large-scale nanophotonic phased array. *Nature* **493**, 195-199 (2013).
- [12] Reed, G.T., Mashanovich, G., Gardes, F.Y. & Thomson, D.J. Silicon optical modulators. *Nature Photon.* **4**, 518-526 (2010).
- [13] Bonneau, D. *et al.* Quantum interference and manipulation of entanglement in silicon wire waveguide quantum circuits. *New J. Phys.* **14**, 045003 (2012).
- [14] Sharping, J.E. *et al.* Generation of correlated photons in nanoscale silicon waveguides. *Opt. Express* **14**, 12388-12393 (2006).
- [15] Clemmen, S. *et al.* Continuous wave photon pair generation in silicon-on-insulator waveguides and ring resonators. *Opt. Express* **17**, 16558-16570 (2009).
- [16] Takesue, H. *et al.* Generation of polarization entangled photon pairs using silicon wirewaveguide. *Opt. Express* **16**, 5721-5727 (2008).
- [17] Azzini, S. *et al.* Ultra-low power generation of twin photons in a compact silicon ring resonator. *Opt. Express* **20**, 23100-23107 (2012).
- [18] Xiong, C. *et al.* Slow-light enhanced correlated photon pair generation in a silicon photonic crystal waveguide. *Opt. Lett.* **36**, 3413-3415 (2011).
- [19] Garay-Palmett, K., U'ren, A., Rangel-Rojo, R., Evans, R. & Camacho-López, S. Ultrabroadband photon pair preparation by spontaneous four-wave mixing in a dispersion-engineered optical fiber. *Phys. Rev. A* **78**, 043827 (2008).
- [20] Chen, J., Lee, K.F. & Kumar, P. Deterministic quantum splitter based on time-reversed Hong-Ou-Mandel interference. *Phys. Rev. A* **76**, 031804(R) (2007).
- [21] Matthews, J.C.F., Politi, A., Stefanov, A. & O'Brien, J.L. Manipulation of multiphoton entanglement in waveguide quantum circuits. *Nature Photon.* **3**, 346-350 (2009).
- [22] Rarity, J.G. & Tapster, P.R. Two-color photons and nonlocality in fourth-order interference. *Phys. Rev. A* **41**, 5139-5146 (1990).
- [23] Ramelow, S., Ratschbacher, L., Fedrizzi, A., Langford, N.K. & Zeilinger, A. Discrete Tunable Color Entanglement. *Phys. Rev. Lett.* **103**, 253601 (2009).
- [24] Pittman, T. *et al.* Can two-photon interference be considered the interference of two photons? *Phys. Rev. Lett.* **77**, 1917-1920 (1996).
- [25] Hong, C.K., Ou, Z.Y. & Mandel, L. Measurement of subpicosecond time intervals between two photons by interference. *Phys. Rev. Lett.* **59**, 2044-2046 (1987).
- [26] Ou, Z.Y. & Mandel, L. Observation of spatial quantum beating with separated photodetectors. *Phys. Rev. Lett.* **61**, 54-57 (1988).
- [27] Pan, J.-W. *et al.* Multiphoton entanglement and interferometry. *Rev. Mod. Phys.* **84**, 777-838 (2012).
- [28] Laing, A. *et al.* High-fidelity operation of quantum photonic circuits. *Appl. Phys. Lett.* **97**, 211109 (2010).
- [29] Azzini, S. *et al.* Stimulated and spontaneous four-wave mixing in silicon-on-insulator coupled photonic wire nano-cavities. *Appl. Phys. Lett.* **103**, 031117 (2013).
- [30] Yao, X.-C. *et al.* Observation of eight-photon entanglement. *Nature Photon.* **6**, 225-228 (2012).
- [31] Yao, X.-C. *et al.* Experimental demonstration of topological error correction. *Nature* **482**, 489-494 (2012).
- [32] Ma, X.-S., Zotter, S., Kofler, J., Jennewein, T. & Zeilinger, A. Experimental generation of single photons via active multiplexing. *Phys. Rev. A* **83**, 043814 (2011).
- [33] Mower, J. & Englund, D. Efficient generation of single and entangled photons on a silicon photonic integrated chip. *Phys. Rev. A* **84**, 052326 (2011).
- [34] Gnan, M., Thoms, S., Macintyre, D., De La Rue, R.M. & Sorel, M. Fabrication of low-loss photonic wires in silicon-on-insulator using hydrogen silsesquioxane electron-beam resist. *Electron. Lett.* **44**, 115-116 (2008).
- [35] Sheng, Z. *et al.* A compact and low-loss mmi coupler fabricated with cmos technology. *IEEE Photon. J.* **4**, 2272-2277 (2012).

Acknowledgements

The authors thank A. Politi for useful discussions, and F. Melloni for experimental assistance. This work was supported by the Engineering and Physical Science Research Council (UK), the European Research Council, the Bristol Centre for Nanoscience and Quantum Information, and the European FP7 project QUANTIP. J.W.S. acknowledges support from the Natural Sciences and Engineering Research Council of Canada. R.H.H. acknowledges a Royal Society University Research Fellowship. V.Z. acknowledges support from the Dutch Foundation for Fundamental Research on Matter. G.D.M. acknowledges the FP7 Marie Curie International Incoming Fellowship scheme. J.L.O'B. acknowledges a Royal Society Wolfson Merit Award. M.G. Thompson acknowledges support from the Toshiba Research Fellowship scheme.

Author contributions

Authors J.W.S. and D.B. contributed equally to this work. J.W.S., D.B., J.G.R., J.L.O'B., and M.G. Thompson conceived of and designed the experiments. J.W.S., D.B., and M.G. Thompson analyzed the data. K.O., N.S., H.Y., N.I., and M.E. fabricated the device. R.H.H., V.Z., C.M.N., and M.G. Tanner built the single-photon detector system. J.W.S., D.B., and G.D.M. performed the experiments. J.W.S., D.B., G.D.M., J.G.R., J.L.O'B., and M.G. Thompson wrote the manuscript.

Competing financial interests

J.W.S., D.B., J.L.O'B., and M.G. Thompson declare UK patent application number 1302895.6. The authors declare no other competing financial interests.